THE JOURNAL OF BIOLOGICAL CHEMISTRY VOL. 283, NO. 4, pp. 2078–2087, January 25, 2008

Getting in Sync with Dimeric Eg5

INITIATION AND REGULATION OF THE PROCESSIVE RUN[*][S]

Received for publication, October 9, 2007, and in revised form, November 20, 2007 Published, JBC Papers in Press, November 25, 2007, DOI 10.1074/jbc.M708354200

Troy C. Krzysiak, Michael Grabe, and Susan P. Gilbert[1]

From the Department of Biological Sciences, University of Pittsburgh, Pittsburgh, Pennsylvania 15260

Eg5/KSP is the kinesin-related motor protein that generates the major plus-end directed force for mitotic spindle assembly and dynamics. Recent work using a dimeric form of Eg5 has found it to be a processive motor; however, its mechanochemical cycle is different from that of conventional Kinesin-1. Dimeric Eg5 appears to undergo a conformational change shortly after collision with the microtubule that primes the motor for its characteristically short processive runs. To better understand this conformational change as well as head-head communication during processive stepping, equilibrium and transient kinetic approaches have been used. By contrast to the mechanism of Kinesin-1, microtubule association triggers ADP release from both motor domains of Eg5. One motor domain releases ADP rapidly, whereas ADP release from the other occurs after a slow conformational change at ~1 s^{-1}. Therefore, dimeric Eg5 begins its processive run with both motor domains associated with the microtubule and in the nucleotide-free state. During processive stepping however, ATP binding and potentially ATP hydrolysis signals rearward head advancement 16 nm forward to the next microtubule-binding site. This alternating cycle of processive stepping is proposed to terminate after a few steps because the head-head communication does not sufficiently control the timing to prevent both motor domains from entering the ADP-bound state simultaneously.

Eg5 is a homotetrameric Bim C/kinesin-5 family member that plays a vital role in the mitotic spindle and has attracted substantial interest as a potential target for chemotherapeutic agents in cancer treatment (1–9). Eg5, as with other members of this subfamily, provides a plus-end directed force necessary to both assemble and organize the mitotic spindle and contributes to microtubule (MT)[2] flux (10–30). If Eg5 function is disrupted prior to anaphase B, the bipolar spindle will collapse into a monoaster from which the cell can no longer divide.

To some extent, the mechanochemistry of dimeric Eg5 appears like conventional Kinesin-1 (referred to as kinesin herein) in that it alternates catalysis on its motor domains to step processively along a MT (31–35) However, dimeric Eg5 only takes 8–10 steps on average (36–38), whereas conventional kinesin can take hundreds (39, 40). The mechanochemical cycle of kinesin is tuned such that it can step processively as soon as the first motor domain touches the MT track. In contrast, Eg5 requires a slow conformational change after MT collision to establish the intermediate poised to begin the processive run (35, 41). The velocity of Eg5 stepping is controlled by the rate of ATP hydrolysis, yet the rate of phosphate release determines the velocity of kinesin (35, 42). These initial studies indicate that the head-head communication used by Eg5 to establish and regulate a processive run is novel, suggesting that Kinesin-5 motors have additional mechanistic requirements that are not yet fully understood.

In this study, equilibrium and transient state kinetic approaches have been used to specifically address the mechanistic events that must occur to establish and coordinate the processive stepping of Eg5. This study has revealed that dimeric Eg5 begins a processive run from a nucleotide-free state with both motor domains associated with the MT. Once in a processive run, ATP binding with ATP hydrolysis signals rearward head advancement for the next step. Dimeric Eg5 processivity is proposed to terminate after a few steps because the head-head communication does not sufficiently control the timing to prevent both motor domains from entering the ADP-bound state simultaneously.

EXPERIMENTAL PROCEDURES

Standard Conditions—The experiments were performed at 25 °C in ATPase buffer: 20 mM Hepes, pH 7.2, with KOH, 5 mM magnesium acetate, 0.1 mM EDTA, 0.1 mM EGTA, 50 mM potassium acetate, 1 mM dithiothreitol. The MTs were stabilized with paclitaxel (Sigma) in Me_2SO. For all mantAXP experiments, a racemate (Invitrogen) was used. Unless otherwise noted, mantAXP was excited at λ_{ex} = 360 nm, and emission at 450 nm was monitored using a 400 nm long pass filter. Monomeric and dimeric Eg5 protein concentrations are reported as single motor domain or active site concentrations.

Cloning of R234K—A pRSETa plasmid with sequence encoding the first 513 amino acids of the human *EG5* gene and a

* This work was supported by NIGMS Grant R01-GM54141 from the National Institutes of Health (to S. P. G.), NIAMS Career Development Award K02-AR47841 from the National Institutes of Health and Department of Health and Human Services (to S. P. G.), and Starter Grant MCB-0722724 from the National Science Foundation (to M. G.). The costs of publication of this article were defrayed in part by the payment of page charges. This article must therefore be hereby marked "*advertisement*" in accordance with 18 U.S.C. Section 1734 solely to indicate this fact.

[S] The on-line version of this article (available at http://www.jbc.org) contains supplemental Figs. S1–S3.

[1] To whom correspondence should be addressed: Dept. of Biology, Rensselaer Polytechnic Institute, Troy, NY 12180-3590. Tel.: 518-276-4415; Fax: 518-276-2851; E-mail: sgilbert@rpi.edu.

[2] The abbreviations used are: MT, microtubule; AMPPNP, adenosine 5′-(β,γ-imido)triphosphate; AXP, ATP, ADP, ATPγS, or AMPPNP; ATPγS, adenosine-5′-(γ-thio)-triphosphate; Eg5-367, a monomeric Eg5 motor consisting of amino acids 1–367 of the human *EG5* gene; $Eg5\text{-}367_{NF}$, Eg5-367 that has been purified without nucleotide; Eg5-513, a dimeric Eg5 motor consisting of amino acids 1–513 of the human Eg5 gene; $Eg5\text{-}513_{NF}$, Eg5-513 that does not contain ADP at its active sites; R234K, Eg5-513 with an arginine to lysine mutation at position 234; mant, 2′(3′)-*O*-(*N*-methylanthraniloyl).

C-terminal His_5 tag was used as the template (36, 43). PCR site-directed mutagenesis using primers 5′-GCATACTCTAGTAAGTCCCACTCAGTTTTC-3′ and 5′-GAAAACTGAGTGGGACTTACTAGAGTATGC-3′ was performed to mutate arginine 234 to lysine. Following PCR, the template was digested with DpnI, and the PCR mixture was used to transform the Nova Blue cell line (EMD Chemicals, Inc.). Sequence-confirmed plasmids were transformed into the BL21-CodonPlus (DE3)-RIL cell line (Stratagene) for protein expression.

Protein Purification—Eg5-513 was purified by MT affinity as described (43). The R234K mutant was purified by a two-step column chromatography method utilizing S-Sepharose ion exchange followed by Ni^{2+}-nitrilotriacetic acid affinity as described (44). Eg5-367_{NF} was purified by column chromatography as described by Cochran and Gilbert (45). Protein concentration was determined using the Bio-Rad protein assay with IgG as the protein standard.

Nucleotide-free Eg5-513—Two methods were used to generate nucleotide-free Eg5-513_{NF}. One method is the treatment of the motor with apyrase (0.02 units/ml; grade VII, Sigma) as described (35). This apyrase isoform catalyzes the conversion of ADP to AMP predominantly. The affinity of Eg5-513 for AMP is so weak that apyrase treatment effectively generates a nucleotide-free state for Eg5. Steady-state experiments were performed using [α-^{32}P]ATP or [α-^{32}P]ADP to monitor the apyrase reaction and kinetics. At the conditions of the Eg5 kinetic experiments, the rate of apyrase conversion of [α-^{32}P]ADP to [α-^{32}P]AMP was 0.01 s^{-1}, and the conversion of [α-^{32}P]ATP to [α-^{32}P]ADP occurred extremely slowly at 0.0002 s^{-1}. Thus, the apyrase does not compete with the Eg5 ATPase kinetics being measured. For the second approach, Eg5-513_{NF} was obtained by supplementing existing protein stocks with 6 mM EDTA followed by gel filtration using a Bio-Spin P-30 column (Bio-Rad) equilibrated in ATPase buffer lacking magnesium acetate and supplemented with 6 mM EDTA. The excluded protein was subjected to a second round of gel filtration in ATPase buffer to remove the EDTA and to adjust the solution back to standard conditions with 5 mM magnesium acetate. Both protocols to obtain nucleotide-free Eg5-513_{NF} yielded kinetics that were indistinguishable experimentally.

Quantification of Tightly Bound ADP by Gel Filtration—Kinesin motors are purified with ADP bound at the active site; therefore, the strategy of this assay is to use gel filtration to quantify the concentration of tightly bound [α-^{32}P]ADP that partitions with Eg5-513 protein (46). Briefly, a 200-μl reaction containing 20 μM Eg5 plus 1 μl of [α-^{32}P]ATP was incubated for 90 min. Three 60-μl aliquots were each applied to Bio-Spin-P-30 columns followed by centrifugation. Free ADP and [α-^{32}P]ADP were included in the resin pores, yet the protein with its tightly bound [α-^{32}P]ADP eluted in the void volume. The volume and protein concentration of the void volume were determined. The concentration of [α-^{32}P]ADP partitioning with Eg5 after gel filtration was determined by spotting aliquots of 1, 2, and 5 μl from the void volume and the starting 200-μl reaction onto thin layer chromatography plates and quantified using a PhosphorImager. Dimeric kinesin K401 and ovalbumin were used as control proteins (46). The ovalbumin 200-μl reaction was supplemented with 20 μM MgADP to evaluate nonspecific [α-^{32}P]ADP partitioning with ovalbumin.

MantADP Titration of Eg5-513 Sites in the Absence of MTs—Equilibrium titration of nucleotide-free Eg5-513_{NF} (EDTA treatment) and Eg5-367_{NF} (0.3–4 μM motor) with mantADP was performed using a FluoroMax-2 spectrofluorometer with magnetic stirring capability (Jobin Yvon-Spex Instruments S.A., Inc). Data were collected using the DataMax software program. The sample was excited at 290 nm, and mantADP emission was monitored at 445 nm. For each mantADP concentration, three trials with an integration time of 1 s were collected and averaged. Both the volume of the sample and the motor active site concentration were constant. The total mantADP concentration was determined for each point i as shown in Equation 1,

$$(V - v) \times (M_{i-1} + v \times m)/V \quad \text{(Eq. 1)}$$

where V is the total volume of the sample; M_{i-1} is the concentration of the sample at the previous point; v is the volume being added, and m is the concentration of the mantADP stock being added. The measured fluorescence intensity was corrected for the inner filter effect (47):

$$F_{i,c} = F_{i,\text{obs}} \times 10^{0.5(Abs_{i,\text{ex}} + Abs_{i,\text{em}})} \quad \text{(Eq. 2)}$$

where $F_{i,c}$ is the corrected fluorescence intensity; $F_{i,\text{obs}}$ is the observed fluorescence intensity; and $Abs_{i,\text{ex}}$ and $Abs_{i,\text{em}}$ are the absorbance of the sample at point i at the excitation and emission wavelengths. The contributions of free mantADP in the buffer solution were subtracted, and the data were fit to either a hyperbola or sum of two hyperbolas (47).

MantADP Release from Head 1 and 2 of Dimeric Eg5—Eg5-513 or R234K was incubated with a 5-fold molar excess of mantADP for 4 h and then subjected to gel filtration to remove ADP and excess mantADP. The protein concentration of the column void volume was determined using the Bio-Rad protein assay. MantADP was then added back to the column void to ensure mantADP was bound at both active sites. The resultant Eg5·mantADP complex was mixed in the KinTek SF2003 stopped flow (KinTek Corp.) with MTs plus 1 mM MgATP. A fluorescence decrease was monitored, and the observed exponential rates were fit to a hyperbola (Fig. 2). To determine the kinetics of mantADP release from the high affinity site, the experiment was repeated using the Eg5·mantADP complex obtained after gel filtration. Typically, ~60% of the sites were labeled with mantADP.

MantATP Binding to Eg5-513_{NF} in the Absence of MTs—Eg5-513 or apyrase-treated Eg5-513_{NF} was mixed with mantATP in the stopped flow (Fig. 3). Final concentrations are as follows: 0.5 μM Eg5-513, 0.0005 units/ml apyrase, and varying mantATP. The observed exponential rates of the fluorescence increase (λ_{ex} = 290 nm, λ_{em} = 450 nm, and 400 nm long pass filter) were fit to a hyperbola.

MantATP Binding during "The Race"—To determine the sequence of events that occurs prior to the slow conformational change, a stopped-flow experiment was designed and referred to here as The Race. Syringe 1 contained Eg5-513, apyrase-treated Eg5-513_{NF}, or Eg5-367_{NF}. Syringe 2 contained MTs and

mantATP. After rapid mixing in the stopped flow, the fluorescence enhancement of mantATP binding to the active site was monitored (Fig. 3).

MantATP Binding to the MT·Eg5-513$_{NF}$ Complex under Single Turnover Conditions—A MT·Eg5-513 complex was treated with apyrase and mixed in the stopped flow with mantATP. Final concentrations are as follows: 15 μM Eg5-513, 25 μM MTs, 1 μM mantATP (Fig. 4).

MantADP Release during Motor Stepping—A MT·Eg5-513$_{NF}$ complex was supplemented with mantATP immediately prior to loading the complex in the stopped flow. The time required to load the stopped-flow instrument was sufficient for Eg5-513$_{NF}$ to bind mantATP, hydrolyze the nucleotide to mantADP·P$_i$, and release P$_i$ (35). The resultant MT·Eg5-513·mantADP complex was then rapidly mixed with MgATP, MgADP, MgATPγS, or MgAMPPNP. Final concentrations are as follows: 15 μM Eg5-513, 25 μM MTs, 1 μM mantADP, 500 μM MgAXP (Fig. 5). The ATP-promoted observed rates of mantADP release were fit to a hyperbola.

MantATP Binding to the MT·R234K Complex—A MT·Eg5-513 complex was treated with apyrase and then rapidly mixed in the stopped flow with mantATP. Final concentrations are as follows: 0.5 μM R234K/8 μM MTs for 0.5–4 μM MgMantATP and 2 μM R234K/8 μM MTs for 4–50 μM MgMantATP (Table 2 and supplemental Fig. S2). The data were fit to the following equation (Equation 3),

$$k_{obs}(K_a k_{max}[\text{mantATP}]/(K_a[\text{mantATP}] + 1)) + k_{off} \quad \text{(Eq. 3)}$$

where K_a represents the equilibrium association constant, k_{max} is the maximum rate constant of the ATP-promoted isomerization that forms the tightly bound mantATP intermediate that proceeds to ATP hydrolysis, and k_{off} is the dissociation of mantATP. The $K_{½,MantATP} = 1/K_a$, and $K_a k_{max}$ represents the second-order rate constant for substrate binding.

Modeling the Kinetics of the Processive Run—The linear kinetic model in the *inset* of Fig. 6 was constructed to attempt to reproduce the time course of mantADP release during the processive run shown in Fig. 5*A*. We followed the initial concentrations in time until the point where mantADP was released and the signal quenched. Experimentally, the system is prepared such that the predominant species is state E5 (Fig. 6). However, the fluorescence decay in the absence of ATP suggests that some dimers have ADP bound at both heads and are in state E0. After several seconds all curves in Fig. 5*A* asymptote to a value that is nearly constant on the time scale of the experiments; therefore, we assume that a fraction of the initial fluorescence signal is constant over time and that the amplitude of this fraction depends on the experimental ATP concentration. There are five free rate constants in the model: k_2, k_3, k_4, and k_5. The rate constant k_5 is a composite rate for species in state E0 to bind to MT, release mantADP, and enter state E2. The concentration-dependent rate of ATP binding to the nucleotide-free head was determined previously by the ATP binding kinetics presented in Ref. 35, where Equation 4 was based on Equation 3,

$$k_1 = 54\ s^{-1} \times 0.11\mu M^{-1}[\text{ATP}]/((0.11\ \mu M^{-1}[\text{ATP}]) + 1) \quad \text{(Eq. 4)}$$

TABLE 1
ADP bound to Eg5-513 after gel filtration

Protein	ADP (μM)/active site (μM)	Range
Eg5-513	0.64 ± 0.01	0.62–0.66
Dimeric kinesin K401	0.92 ± 0.02	0.83–1
Ovalbumin	0.01 ± 0.002	0.001–0.013
Eg5-513 + 1 mM MgADP	0.59 ± 0.04	0.44–0.74

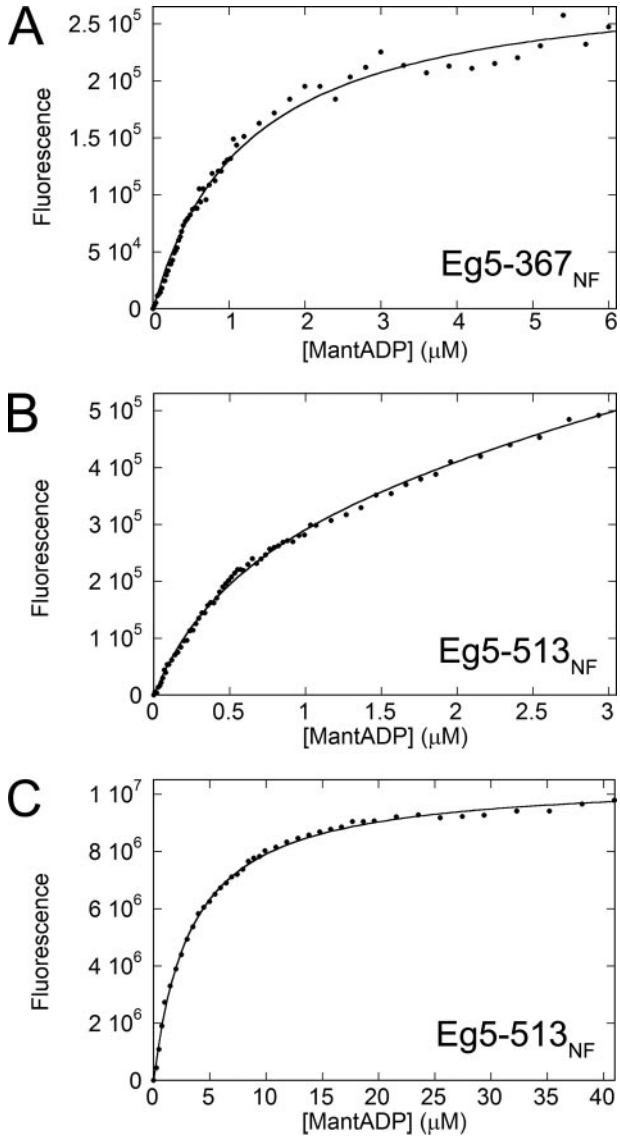

FIGURE 1. **MantADP titration of Eg5 motors free in solution.** Titrations of nucleotide-free monomeric and dimeric Eg5 motors were performed at constant volume and motor concentration. *A*, 300 nM monomeric Eg5-367$_{NF}$ was titrated with mantADP. The resultant increase in fluorescence was best fit by a single hyperbola yielding an apparent $K_{d,mantADP}$ = 1.2 ± 0.1 μM. *B*, 300 nM dimeric Eg5-513$_{NF}$ was titrated with mantADP. The resultant increase in fluorescence was best fit by a sum of two hyperbolas yielding an apparent $K_{d,mantADP}$ = 0.62 ± 0.14 μM for the initial phase. *C*, 4 μM dimeric Eg5-513$_{NF}$ was titrated with mantADP. The resultant increase in fluorescence was best fit by a single hyperbola yielding an apparent $K_{d,mantADP}$ = 3.3 ± 0.1 μM.

The initial concentration of molecules in states E5 and E0 and the value of the constant background fluorescence provided two more free parameters per curve in Fig. 5*A*. We systematically searched for a single set of rate constants that described all of the curves in Fig. 5*A*. For each set of initial conditions and a given ATP concentration, the kinetic model was solved using

TABLE 2
Dimeric Eg5-513 and R234K constants based on model presented in Fig. 6

	Experimentally determined Eg5-513	Experimentally determined Eg5-R234K	Intrinsic constants Eg5-513[a]
MT·Eg5 association			
k_{+1}	2.8 ± 0.2 μM^{-1} s^{-1} [b]	26 ± 2.3 μM^{-1} s^{-1}	
k_{-1}	9.7 ± 1 s^{-1}	24 ± 13 s^{-1}	
ADP release head 1			
k_{+1}	28 ± 0.5 s^{-1}	20 ± 0.9 s^{-1}	
Slow structural transition			
k_{+2}	~1 s^{-1}	~1 s^{-1}	1.2 s^{-1}
ADP release head 2			
k_{+2}	0.62 ± 0.04 s^{-1}	0.79 ± 0.04 s^{-1}	
Mant-ATP binding[c]			
$K_3k_{+3'}$	5.8 μM^{-1} s^{-1} [b]	8.4 μM^{-1} s^{-1}	
$k_{+3'}$	54 ± 3 s^{-1}	77 ± 3.0 s^{-1}	
$K_{½,mant\text{-}ATP}$	9.4 μM	9.1 μM	
ATP hydrolysis			
k_{+4}	5–10 s^{-1} [b]	0.08 ± 0.003 s^{-1}	10.7 s^{-1}
Pi release coupled to			
Rearward head	6.6 ± 3 s^{-1} [b]	ND[d]	
Detachment k_{+5}	$K_{½,ATP}$ = 5.4 ± 1.3 μM		
Steady-state parameters			
k_{cat}	0.5 ± 0.02 s^{-1} [e]	0.02 ± 0.01 s^{-1}	
$K_{m,ATP}$	7.9 ± 2.4 μM	ND	
$K_{½,MT}$	1.8 ± 0.2 μM	ND	

[a] Data are based on computer modeling.
[b] Data are from Krzysiak and Gilbert (35).
[c] Data are from Equation 3.
[d] ND means not determined.
[e] Data are from Krzysiak *et al.* (43).

the ordinary differential equations function ODE15 in Matlab. This was repeated for all six transients, and the root mean square differences of the model solution *versus* the experimental data were calculated for each curve. The root mean square difference was then used as a fitness function in a Nelder-Mead search algorithm to determine the parameter set that maximized the goodness of the fit (48). Initial rates and values were chosen from a reasonable domain with a random number generator, and well over 100,000 sets of parameters were searched. The best fit is shown in Fig. 5*C*, and the corresponding values are presented in the legend of Fig. 5.

RESULTS

Our initial kinetic analysis of Eg5-513 suggested that steady-state ATP turnover by dimeric Eg5 is governed by a slow structural transition (35, 43). This slow conformational change occurs after collision with the MT but prior to processive stepping (35, 36). To dissect the sequence of events required to establish the processive run, an analysis of Eg5-513 in the absence of MTs was pursued to assess whether the motor domains of the Eg5 dimer were identical in their affinity for ADP as observed for dimeric kinesin K401. Gel filtration and mantADP titration experiments were used to examine the ADP affinity.

Eg5-513 Has an Asymmetric ADP Affinity while Free in Solution—Eg5-513 was incubated with trace [α-^{32}P]ATP to exchange the ADP that copurifies with the motor with [α-^{32}P]ADP after hydrolysis and subjected to gel filtration. Only [α-^{32}P]ADP tightly bound to the active site will accompany the motor through the column. Table 1 shows that 64% of Eg5 active sites retained ADP, whereas dimeric kinesin K401 held ADP at almost all of its sites (92%), consistent with previous reports (49, 50). Ovalbumin showed very low nonspecific binding of [α-^{32}P]ADP as expected for a protein without a nucleotide-binding site. Furthermore, when Eg5-513 was incubated with an additional 1 mM MgADP prior to gel filtration, additional active sites were not observed to contain ADP (Table 1).

These data lead to two possible interpretations. 1) There is a distinct difference in affinity for ADP between the two motor domains of the dimer, or 2) the affinity for ADP at each site is similar, and the gel filtration result reflects a shared ADP affinity. To distinguish between these two possibilities, mantADP titration experiments were performed, comparing monomeric and dimeric Eg5 motors (Fig. 1). The mantADP binding curve for monomeric Eg5-367$_{NF}$ at 300 nM was monophasic with an apparent $K_{d,mantADP}$ = 1.6 μM (Fig. 1*A*). In contrast, titration of dimeric Eg5-513$_{NF}$ at 300 nM reveals a biphasic binding curve with an apparent $K_{d,mantADP}$ of 0.5 μM for the higher affinity or tighter site (Fig. 1*B*). To obtain a more accurate dissociation constant for the weaker site, titrations were performed at 4 μM Eg5-513$_{NF}$. The biphasic appearance of the mantADP binding is lost at the higher enzyme concentration, and the fit of the data provides an apparent $K_{d,mantADP}$ = 3.3 μM for the second site that binds ADP more weakly (Fig. 1*C*).

These results indicate that dimeric Eg5 in solution shows an asymmetry in nucleotide affinity in that one head holds ADP tightly, whereas the partner head binds ADP more weakly. This is an intriguing observation because it implies that there is head-head communication in the Eg5 dimer prior to its interaction with the MT. Furthermore, we find that half-site behavior of dimeric Eg5-513 consistently shows ~60% high affinity sites rather than the 50% expected for a homogeneous popula-

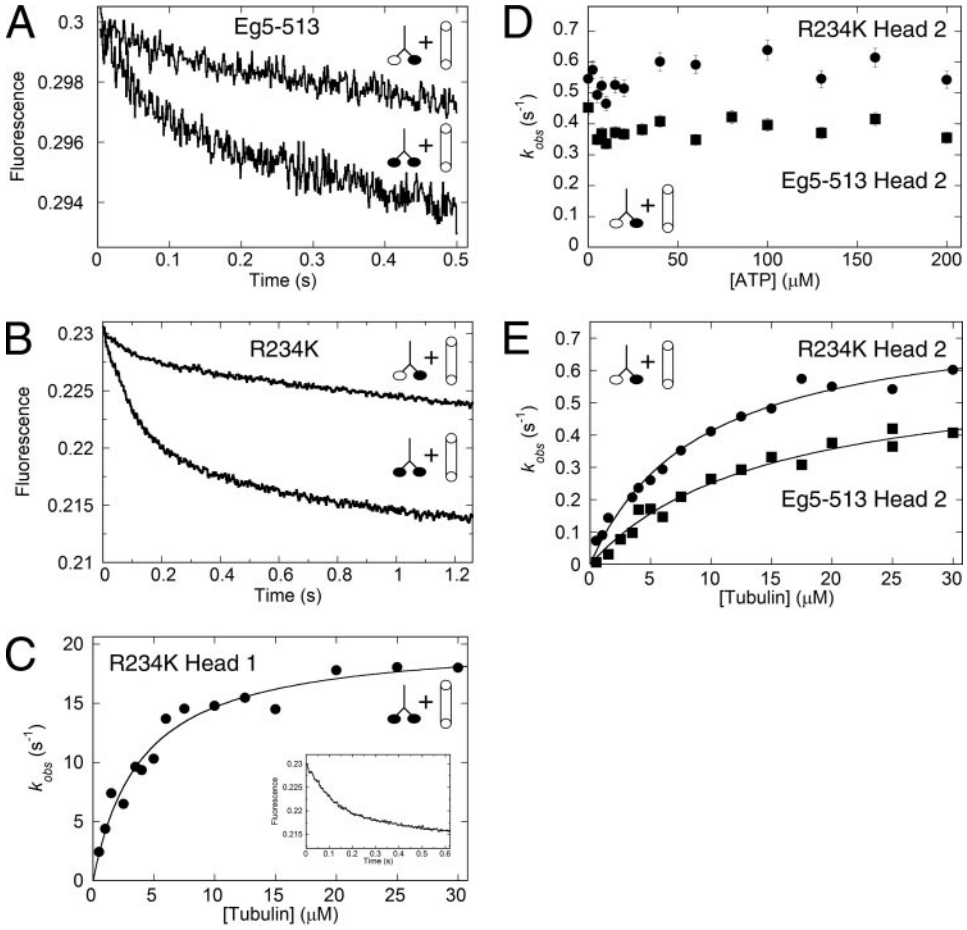

FIGURE 2. **ADP release from head 2.** The Eg5-513·mantADP or R234K·mantADP complex was preformed with mantADP on both motor domains (1:1) or predominantly on one motor domain (1:0.6). The complex was then rapidly mixed in the stopped-flow instrument with MTs plus MgATP. *A*, representative transients of Eg5-513 mantADP release. (Final mixture: 2 μM Eg5-513, 10 μM MTs, 500 μM MgATP.) *B*, representative transients of R234K mantADP release. (Final mixture: 2 μM R234K, 4 μM MTs, 500 μM MgATP.) *C*, observed rates for R234K·mantADP of the initial fast phase plotted as a function of MT concentration: $k_{max} = 20.4 \pm 0.9\ s^{-1}$, $K_{1/2,MTs} = 3.9 \pm 0.5\ \mu M$. *Inset*, representative transient obtained from mixing a R234K·mantADP complex with MTs + MgATP (final mixture: 5 μM MTs). *D*, an Eg5-513·mantADP (■) or an R234K·mantADP complex (●) with mantADP at one active site was mixed with MTs and varying MgATP. Final mixture: 2.5 μM motor, 25 μM MTs. The observed rate of mantADP release from head 2 did not increase as a function of increasing MgATP concentration. *E*, experiment was repeated but as a function of increasing MT concentration, and each data set was fit to a hyperbola as follows: Eg5-513 (■), $k_{max} = 0.62 \pm 0.04\ s^{-1}$, $K_{1/2,MTs} = 14.6 \pm 2.3\ \mu M$, and R234K (●) $k_{max} = 0.79 \pm 0.04\ s^{-1}$, $K_{1/2,MTs} = 9.1 \pm 1\ \mu M$. (Final mixture: 2 μM Eg5-513 or R234K, varying MTs, 500 μM MgATP.)

tion with one tight-binding site. This result may be due to the difficulty in obtaining an accurate protein determination, a population averaging effect in which some dimers exhibit a conformation that would hold ADP tightly at both sites, and/or the result of the equilibrium that results with a high ADP affinity site and a low ADP affinity site.

Head-Head Communication and MantADP Release—Our previous study of mantADP release kinetics indicated biphasic release with the first exponential phase at 28 s^{-1} and the second phase at 0.5 s^{-1} (35) (Table 2). These data are consistent with a model in which the initial exponential phase represents the first motor head colliding with the MT followed by mantADP release, and the second slower phase represents mantADP release from the second head but after the slow conformational change that was limiting steady-state ATP turnover. Interestingly, in this previous study, we also observed that the rate of mantADP release from the second head appeared to be dependent upon the concentration of MTs in the experiment (see Fig. 8 in Ref 35). This observation suggests that the head-head communication for Eg5 may be different from the signaling mechanism for kinesin in which MT concentration only affects the rate of mantADP release from head 1, and it is ATP binding at kinesin head 1 that triggers forward stepping and mantADP release from head 2 (33–35, 51, 52).

To explore what defines the signal for the second motor domain to bind the MT and release its ADP in Eg5, we devised a series of experiments that looked carefully at mantADP release from each head of the Eg5 dimer. We engineered an Eg5-513 mutant, R234K, that was defective for ATP hydrolysis, yet with the other steps in the ATPase cycle relatively similar to wild type Eg5-513 (Supplemental Material and Table 2). Eg5-513 or R234K was incubated with mantADP either to label both sites with mantADP or to label one site with mantADP. The Eg5·mantADP complex was then rapidly mixed in the stopped-flow instrument with MTs plus MgATP, and the kinetics of mantADP release were monitored (Fig. 2, *A* and *B*). When both heads of the dimer were labeled with mantADP, the kinetics were biphasic for both Eg5-513 and R234K. To measure the mantADP kinetics from the high affinity site of the dimer, gel filtration was used to remove weakly bound mantADP. Upon collision with MTs, the mantADP release kinetics were also biphasic, but the slower second phase predominated with the initial rapid phase representing only a small fraction of the total amplitude (Fig. 2, *A* and *B*). Fig. 2*C* shows for R234K that the rate of mantADP release from head 1 upon MT collision increased as a function of increasing MT concentration, $k_{max} = 20\ s^{-1}$, which is similar to the rate of mantADP release obtained for wild type Eg5-513 at 28 s^{-1} (Table 2) (35). To evaluate whether ATP and/or ATP hydrolysis signaled head 2 to bind the MT as observed for dimeric kinesin (33, 34), Eg5-513 and R234K were labeled with mantADP followed by gel filtration to generate the Eg5 dimer with mantADP only on the high affinity site of head 2 (Fig. 2*D*). Eg5 was rapidly mixed in the stopped-flow with 25 μM MT plus MgATP, and the kinetics of mantADP release from head 2 were monitored. Surprisingly, the rate did not change for either Eg5-513 or R234K as a function of ATP concentration, suggesting that ATP binding or ATP hydrolysis did not modulate mantADP

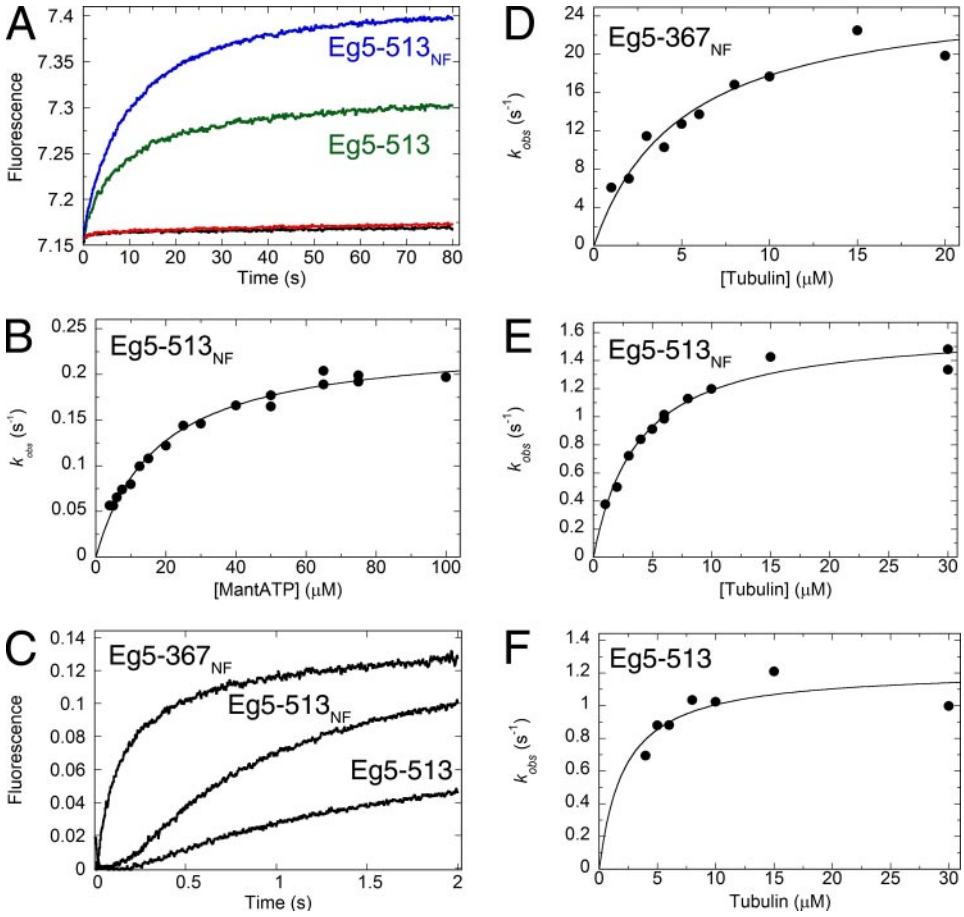

FIGURE 3. **ATP binding follows MT·Eg5 association.** *A*, averaged transients representing the fluorescence enhancement upon mixing Eg5 with mantATP in the absence of MTs: nucleotide-free Eg5-513$_{NF}$ (*blue*, apyrase-treated), Eg5-513 as purified (*green*), apyrase in the absence of motor (*red*), or buffer with mantATP (*black*). Final mixture: 0.5 μM Eg5-513, $\pm$0.005 units/ml apyrase, 75 μM MgMantATP. *B*, observed rate of the initial exponential phase increased as a function of increasing mantATP concentration, $k_{max} = 0.23 \pm 0.12\ s^{-1}$; $K_{1/2,mantATP} = 14.5 \pm 2.4\ \mu M$. *C–F*, Eg5 was mixed in the stopped-flow instrument with MTs plus MgMantATP. Final mixture: 3 μM motor, 30 μM MgMantATP, and varying MTs. *C*, comparison of the mantATP binding kinetics for each motor (final mixture: 8 μM MTs). The observed rate of the initial fast phase for mantATP binding increased as a function of increasing MT concentrations. *D*, Eg5-367$_{NF}$ $k_{max} = 26.8 \pm 2.3\ s^{-1}$, $K_{1/2,MT} = 5.1 \pm 1.1\ \mu M$. *E*, Eg5-513$_{NF}$ $k_{max} = 1.6 \pm 0.1\ s^{-1}$, $K_{1/2,MT} = 3.8 \pm 0.4\ \mu M$. *F*, Eg5-513 $k_{max} = 1.2 \pm 0.1\ s^{-1}$, $K_{1/2,MT} = 2.1 \pm 1\ \mu M$.

release from head 2 in this experimental design. However, when the experiment was repeated but at varying MT concentrations plus 1 mM MgATP (Fig. 2*E*), the rate of mantADP release increased as a function of increasing MT concentrations for both Eg5-513 ($k_{max} = 0.62\ s^{-1}$) and R234K ($k_{max} = 0.79\ s^{-1}$). These results indicate that Eg5 begins its ATPase cycle by head 1 colliding with the MT and releasing ADP rapidly, followed by a slow conformational change at $\sim$1 s^{-1} that limits ADP release from head 2 (Fig. 6, *steps 1* and *2*).

The Race—The results presented in Fig. 2 indicated that collision with the MT was sufficient to release ADP from both motor domains, suggesting that both heads are bound to the MT and nucleotide-free prior to ATP binding (Fig. 6, *species E2*). However, these experiments did not provide information to order the steps of ATP binding and the slow $\sim$1 s^{-1} conformational change required to establish the processive run. A novel stopped-flow experiment called The Race was designed to define the sequence of events from MT collision to ATP binding and to ask whether ATP binding or MT binding occurred first. This experimental design required mantATP binding to Eg5 in solution to be slow (Fig. 3, *A* and *B*), mantATP binding for the MT·Eg5 complex to be rapid (54 s^{-1}; Table 2), and MT-Eg5 association to be rapid (2.8 $\mu M^{-1}s^{-1}$; Table 2). Fig. 3*A* shows representative transients of mantATP binding to Eg5-513 and Eg5-513$_{NF}$ in the absence of MTs. The amplitude associated with the kinetics of Eg5-513$_{NF}$ is higher than Eg5-513 as expected because Eg5-513 retains ADP at $\sim$60% of its sites. Fig. 3*B* shows that mantATP binding in the absence of MTs is very slow at 0.23 s^{-1}. For The Race (Fig. 3*C*), Eg5 is loaded in one syringe, and the second syringe contains MTs plus mantATP. (Final concentrations after mixing were 3 μM Eg5, 8 μM MTs, 30 μM mantATP.) At these concentrations, mantATP binding to Eg5 would occur at $\sim$0.15 s^{-1} in solution but at $\sim$40 s^{-1} if the Eg5 head were already bound to the MT (35, 44). At 8 μM MTs, MT association is rapid and >20 s^{-1} (35, 44). For monomeric Eg5-367$_{NF}$, mantATP binding was immediate and rapid, indicating that the motor head bound the MT first followed by rapid mantATP binding. In contrast, for both dimeric Eg5-513$_{NF}$ and Eg5-513, there was a lag prior to mantATP binding to the active site.

When The Race was repeated with increasing MT concentrations, the rate of mantATP binding increased to a maximum of 27 s^{-1} for monomeric Eg5-367$_{NF}$ (Fig. 3*D*), yet was 1.6 s^{-1} for Eg5-513$_{NF}$ or 1.2 s^{-1} for Eg5-513 (Fig. 3, *E* and *F*). These rates were significantly slower than mantATP binding to the preformed MT·Eg5-513 complex at 54 s^{-1} (Table 2), but they were similar to the rate of the slow conformational change at $\sim$1 s^{-1}. These results indicate that the slow conformational change occurs after MT collision and is a required structural transition for mantATP to bind to Eg5. Furthermore, the mantATP binding kinetics for Eg5-513 and Eg5-513$_{NF}$ are similar, providing confidence that we are detecting the normal sequence of events that occurs to establish the Eg5 intermediate poised for processive stepping (Fig. 6, *species E2*).

Gating Mechanism during Processive Stepping—Our previous studies indicated that ATP hydrolysis at 5–10 s^{-1} is the rate-limiting step during a processive run (35). Thus, the conformational change that is rate-limiting for the initialization of the processive run cannot occur during subsequent stepping. The new results presented in Figs. 2 and 3 indicate that the slow $\sim$1 s^{-1} structural transition occurs after MT association and

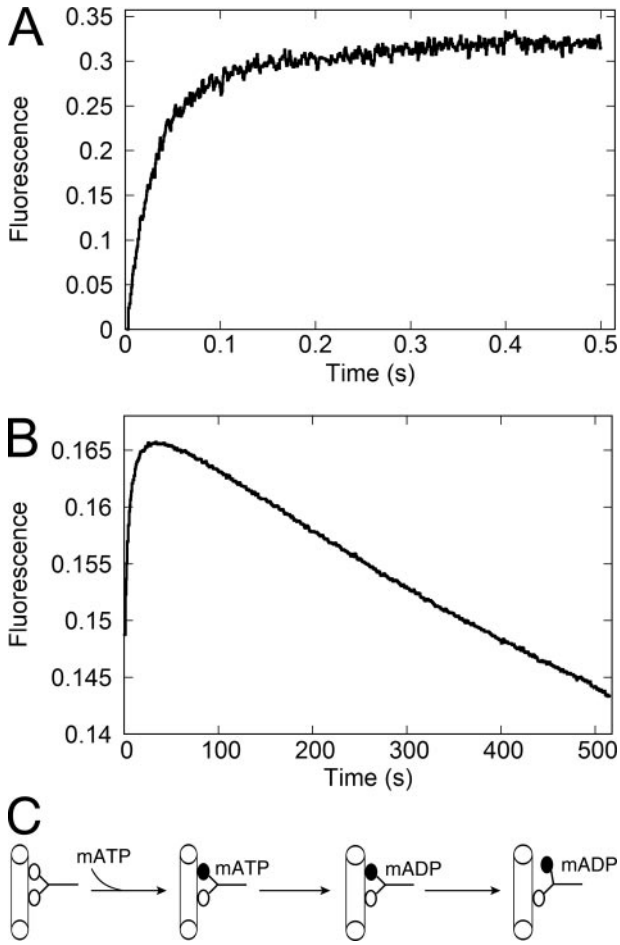

FIGURE 4. **MantATP binding under single turnover conditions.** A preformed MT·Eg5-513$_{NF}$ complex was rapidly mixed in the stopped-flow instrument with mantATP. Final mixture: 15 μM Eg5-513$_{NF}$, 25 μM MTs, 1 μM MgMantATP (*A*) or 0.25 μM MgMantATP (*B*). *A*, representative transient reflecting initial rapid mantATP binding by Eg5-513$_{NF}$: phase 1 $k_{obs} = 33 \pm 0.3$ s^{-1}; phase 2 $k_{obs} = 2.1 \pm 0.06$ s^{-1}. *B*, rapid mantATP binding to the MT·Eg5-513$_{NF}$ complex followed by fluorescence decay with $k_{obs} = 0.0008 \pm 0.00002$ s^{-1}. *C*, experimental design to establish the processive stepping Eg5 intermediate.

prior to ATP binding, which is consistent with this model. However, the question of how the heads of the Eg5 dimer are coordinated during a processive run remains.

To address this question experimentally, we preformed an MT·Eg5-513 complex and treated with apyrase to remove ADP. The MT·Eg5-513$_{NF}$ complex was rapidly mixed with mantATP in the stopped-flow instrument at single turnover conditions (Fig. 4; final concentrations: 15 μM Eg5-513, 25 μM MTs, 1 μM mantATP). MantATP binding resulted in an initial rapid phase of fluorescence enhancement, $k_{obs} = 33$ s^{-1}. However, the fluorescence did not begin to decrease until 50 s elapsed, and the rate was extremely slow at $k_{obs} = 0.001$ s^{-1} (Fig. 4*B*). This observed rate is comparable with the rate of fluorescence decay for mantATP mixed with buffer in the absence of Eg5 or MTs ($k_{obs} = 0.0014$ s^{-1}; data not shown). For kinesins, there is no change in fluorescence associated with mantATP hydrolysis. Therefore, the kinetics in Fig. 4*B* suggest that a long lived Eg-513·mantADP intermediate was formed (Fig. 4*C*), and a nucleotide-gated mechanism prevented rapid mantADP release. Because the ADP state promotes weak Eg5 binding to the MT, we propose that the head holding mantADP is detached from the MT but tethered by the nucleotide-free head that is bound tightly to the MT (Fig. 4*C*).

In the next series of experiments, we used this kinetically stable MT·Eg5-513·mantADP intermediate (Fig. 4*C*) to determine the nucleotide signal that triggers mantADP release during processive stepping (Fig. 6, *steps 6* and *7*). The kinetically stable MT·Eg5-513·mantADP intermediate (Fig. 6, *E5*) was formed by adding mantATP to a MT·Eg5-513$_{NF}$ complex just prior to loading in the stopped-flow instrument. This complex was then rapidly mixed with MgATP in the stopped-flow instrument, resulting in a rapid exponential quenching correlated with mantADP release from the active site (Fig. 5*A*). The initial exponential rate of mantADP release increased as a function of increasing MgATP concentration with $k_{max} = 8.4$ s^{-1} (Fig. 5, *A* and *B*). These results are consistent with rate-limiting ATP hydrolysis on the rearward head at ~10 s^{-1}, followed by rapid MT association and ADP release from the advancing head (35).

Note that the transients in Fig. 5*A* appear biphasic, where the exponential rate for the second slow phase is ATP-independent and occurs at ~1 s^{-1} (Fig. 5*B*). The design of the experiment should result in single exponential kinetics because only one head of the Eg5 dimer should be occupied by mantADP. We do not know the origin of this second phase. It may reflect an off pathway isomerization of mantADP. Alternatively, there may be a population of dimers with mantADP at both sites and free in solution detached from the MT. Upon mixing in the stopped-flow instrument, this population would form the nucleotide-free MT·Eg5-513 species poised to begin a processive run (Fig. 6, *E2*) with the second phase in the Fig. 5*A* transients reflecting the slow ~1 s^{-1} conformational change.

To assess whether ATP binding was sufficient to stimulate mantADP release or whether ATP hydrolysis was required, the stable MT·Eg5-513·mantADP immediate was mixed with the slowly hydrolyzable analogue, ATPγS, and the nonhydrolyzable analogue, AMPPNP (Fig. 5*D*). For both ATP analogues, there was an initial rapid fluorescence decrease ($k_{obs} = 20$–30 s^{-1}) of very small amplitude followed by a slow phase. This slow phase was of comparable amplitude to the slow phase of the ATP transient. The same experiment was also performed using the ATP hydrolysis defective mutant R234K. With AMPPNP, there was almost no initial fast phase, yet the transient for R234K with ATP mimicked the results of mixing MT·Eg5-513·mantADP with AMPPNP or ATPγS.

These results are difficult to interpret for a clear understanding of the gating mechanism. If ATP binding were sufficient in the absence of ATP hydrolysis for forward head advancement, MT association, and mantADP release, we would expect the amplitudes of the AMPPNP, ATPγS, and R234K transients to be equal to the ATP transient in Fig. 5*C* as observed previously for kinesin (34). However, if ATP binding followed by ATP hydrolysis were required for mantADP release, our expectation would be almost no amplitude associated with the AMPPNP, ATPγS, and R234K transients as observed for *Drosophila* Ncd (46). Our interpretation is that the results in Fig. 5*D* indicate that ATP binding is sufficient to induce some of the structural transitions required for forward advancement of the rearward

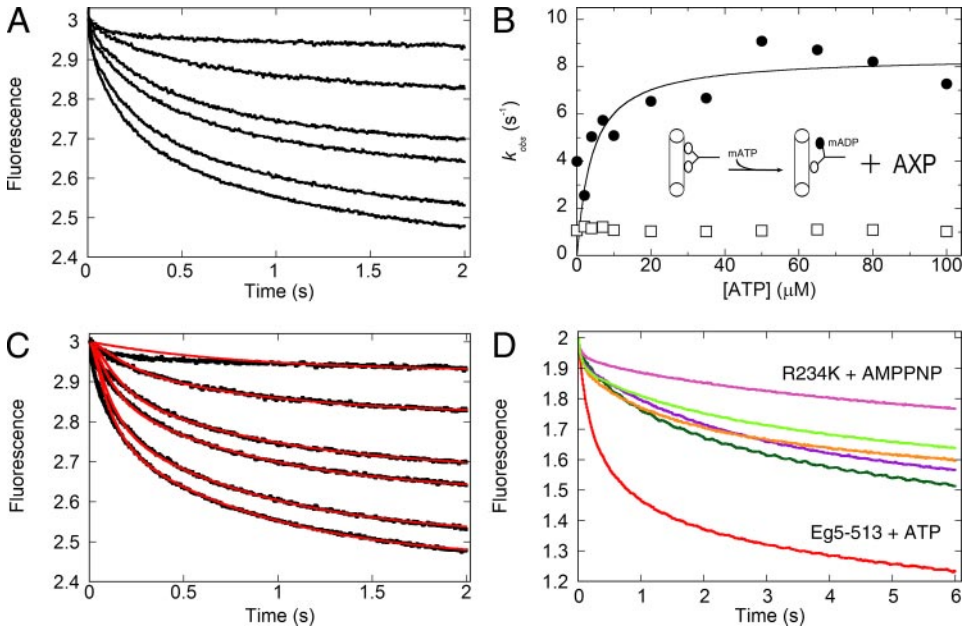

FIGURE 5. **ATP-triggered mantADP release.** A preformed MT·Eg5-513·mantADP complex (see Fig. 4*C*) was mixed in the stopped-flow instrument with MgATP. Final mixture: 15 μM motor, 25 μM MTs, 1 μM mantATP, varying MgATP. *A*, representative transients with MgATP at 0, 2, 4, 10, 20, and 65 μM (*top to bottom*). *B*, observed rate of the initial exponential phase (●) of mantADP release increased as a function of increasing ATP concentration: $k_{max} = 8.4 \pm 0.8\ s^{-1}$, $K_{1/2,ATP} = 4 \pm 1.8$ μM. The second, slower phase (□) at ~1 s^{-1} does not show an ATP concentration dependence. *C*, kinetic model in Fig. 6 (*inset*) was solved numerically for various ATP concentrations and matched to the experimental data in *A*. The rate constants corresponding to the fit shown are as follows: $k_1 = 54\ s^{-1} \times 0.11\ \mu M^{-1}$ [ATP]/((0.11 μM^{-1} [ATP]) + 1); $k_2 > 185\ s^{-1}$; $k_3 = 10.7\ s^{-1}$; $k_4 > 185\ s^{-1}$; and $k_5 = 1.2\ s^{-1}$. *D*, comparison of the kinetics of mantADP release when either a MT·Eg5-513·mantADP or a MT·R234K·mantADP complex was mixed with ATP, ATPγS, or AMPPNP: Eg5-513+ATP (*red*), Eg5-513 + ATPγS (*dark green*), Eg5-513 + AMPPNP (*purple*), R234K + ATP (*orange*), R234K + ATPγS (*light green*), and R234K + AMPPNP (*pink*).

head for MT association and ADP release, yet to achieve the tightly bound, no nucleotide state as illustrated by intermediate E7 requires ATP hydrolysis (Fig. 6, *steps 6* and *7*, and see under "Discussion").

Modeling the Processive Run—Finally, we wanted to return to the processive run data in Fig. 5*A* to determine whether the linear sequence of events presented in Fig. 6 could capture this behavior and the correct dependence on ATP concentration. We see from the solution of the model equations (Fig. 5*C, red lines*) that the scheme presented in Fig. 6 fits the experimental data quite well. Importantly, the rate of ATP binding (rate k_1 in Fig. 6, *inset*) was previously determined in Ref. 35 and was not a free parameter in our model. Nonetheless, the model described the sharp increase in the initial rate of ADP release as ATP is increased. The exact order of events shown in Fig. 6, *inset*, is not known. For instance, we do not know if ATP hydrolysis on head 1 precedes ADP release on head 2 or vice versa, and the modeling does not discriminate between these possibilities. However, three pieces of information concerning the rate constants do emerge from the global fits to the data. First, the rate constant (k_5) associated with free Eg5, state E0, binding to the MT and entering state E2 is 1.2 s^{-1}, which is consistent with the slow conformational change observed after Eg5 collides with the MT (Step 2, Table 2) (35, 41, 43). Second, the modeling revealed that one of the steps following ATP binding occurs at a rate of 10.7 s^{-1}. We associate this step with the rate of ATP hydrolysis based on the previously determined rate-limiting step of ATP hydrolysis (35). Third, the fluorescence signal loses amplitude immediately at the time of mixing without any observable lag, which implies that any intervening steps between ATP binding and mantADP release must be fast. We estimate that these intervening steps such as the head binding to the MT (k_2) and ADP release (k_4) must each be faster than 185 s^{-1}.

DISCUSSION

Initiation of the Processive Run—For kinesin, a processive run begins when a motor head collides with the MT and releases ADP. In contrast, dimeric Eg5 must first establish the intermediate to initiate the processive run (Fig. 6, *steps 1* and *2*). The results in Fig. 1 (mantADP titration) revealed that in solution, one active site holds ADP tightly, whereas the other site binds ADP more weakly. We propose that the cycle begins with the weak head colliding with the MT and releasing its ADP rapidly (Fig. 6, *step 1*). This hypothesis is consistent with the observed 10-s^{-1} off rate in the MT association kinetics (Table 2) (35), suggesting that the head that holds ADP tightly may not bind the MT as readily as the head that holds ADP weakly. An off rate in the MT-motor association kinetics was also observed for dimeric Ncd, which also possesses a high affinity site and a low affinity ADP site (53). In contrast, dimeric kinesin and monomeric Eg5 show no MT association off rate (32, 44). The experiments presented cannot distinguish the orientation of the tethered ADP head of intermediate E1; therefore, we present two possible orientations of the detached head as follows: already forward in its diffusional search for the next MT-binding site as well as detached and rearward to the nucleotide-free head. The results also indicate that the E1 intermediate is unique and distinct from the E5 state because if E1 and E5 were comparable, ATP binding and processive stepping would begin from the E1 intermediate. This is an important observation about the E1 state.

We propose that the slow ~1 s^{-1} conformational change occurs as step 2, resulting in the partner head binding the MT and releasing its ADP to form the intermediate with both heads bound and both nucleotide-free (Fig. 6, *species E2*). The data that support this sequence of events are the observations that mantADP release from the high affinity site is limited by a 0.6–1-s^{-1} event (Fig. 2) (35) and that ATP binding after MT association (Fig. 3) is limited by a 1.2–1.6-s^{-1} event. Based on the fluorescence resonance energy transfer studies of Rosenfeld *et al.* (41) using monomeric Eg5, we propose that the ~1 s^{-1} event in dimeric Eg5 represents reorientation of the ordered neck linker from a position perpendicular to the long axis of the

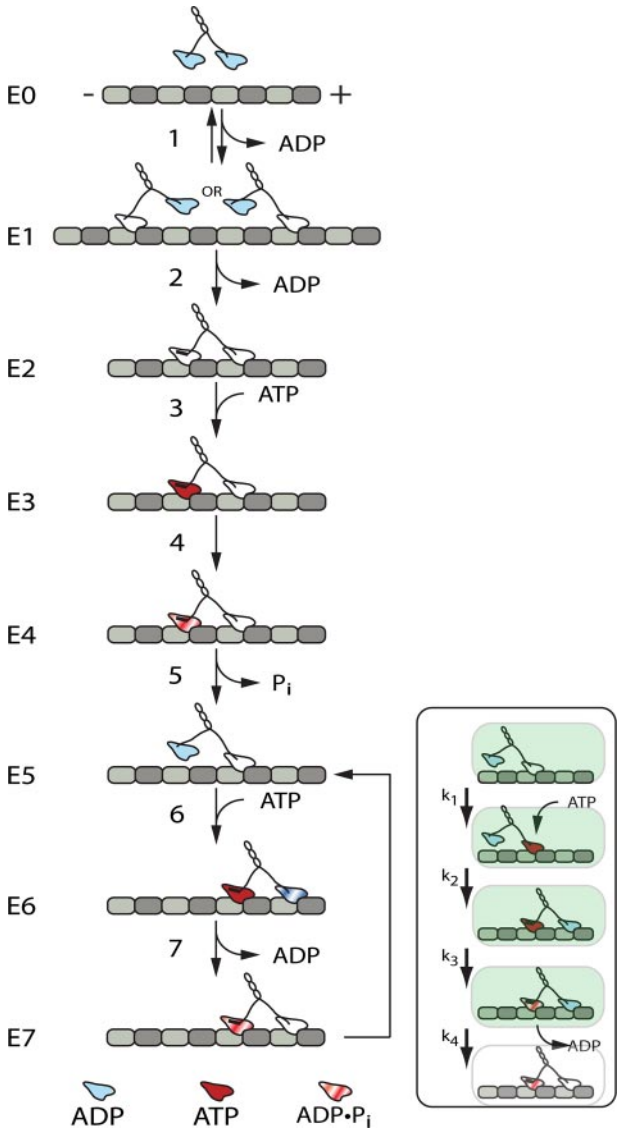

FIGURE 6. **Model of Eg5-513 stepping.** The mechanochemical cycle of dimeric Eg5 has two distinct phases, establishing the competent intermediate for a processive run and the processive run. The cycle begins with the Eg5 dimer in solution with one head holding ADP tightly and the other with ADP more weakly bound. These results indicate that the E0 dimer in solution exhibits head-head communication prior to interaction with the microtubule. In the first step, one head of the Eg5 dimer collides with the MT with rapid ADP release, followed by a slow $\sim 1\ s^{-1}$ conformational change. This conformational change, proposed to be neck linker reorientation, must occur prior to ADP release from the partner motor domain (*steps 1* and *2*) and prior to ATP binding (*step 3*). Intermediate E2 has both motor domains bound to the MT with both active sites nucleotide-free and the neck linkers strained. Processive stepping begins with ATP binding to the rearward head with its neck linker docked approximately parallel with the MT. ATP hydrolysis follows with rapid release of P_i and rearward head detachment. ATP binding and ATP hydrolysis at the forward motor domain (*steps 6* and *7*) are necessary to complete the 16 nm advance of the rearward head toward the MT plus-end, resulting in ADP release and tight binding of the forward head to the MT. Release of P_i at the rearward head returns the E7 intermediate to E5 for another ATP turnover during the processive run. The kinetic scheme in the *inset* was simulated to produce the curves in Fig. 5*C*.

motor to a docked configuration (54, 55), approximately parallel with the MT (species E2). What is unique for Eg5 is that it will begin its processive run from an intermediate with both heads bound to the MT and both free of nucleotide.

The Processive Run—By analogy to kinesin, we propose that the neck linkers of species E2 are strained, which would favor ATP binding at the rearward head because of its docked neck linker configuration (43, 52, 56–58). ATP hydrolysis and phosphate release result in the weakly bound ADP state, leading to rearward head detachment (species E5). However, for the rearward head of species E5 to advance forward toward the MT plus end, ATP must bind and possibly hydrolyze at the forward head (Fig. 5). Once the rearward head steps forward and collides with the MT, ADP is released rapidly. The observed rate constant for ADP release in this experimental design was $8.4\ s^{-1}$, indicative that ATP hydrolysis was controlling the rate of Eg5 stepping during its processive run.

In the next ATP cycle (steps 6 and 7), we propose that ATP binding at the forward head during the processive run results in rapid movement of the neck linker to the docked configuration followed by a MT plus-end directed advancement of the rearward head to the next MT-binding site 8 nm ahead of the ATP-bound head. The results from Figs. 4 and 5 indicate that during processive stepping, ATP binding and ATP hydrolysis at the forward head are required for rearward head advancement to generate the tightly bound E7 intermediate (35, 36, 38). This model accounts for the exceedingly slow steady-state ATP turnover at $0.5\ s^{-1}$, yet at the same time it is consistent with the velocity measurements from the single molecule results of Valentine *et al.* (36–38) at $12\ s^{-1}$. Further support comes from the simulations of the kinetics shown in Fig. 5*C*. This model predicts ATP hydrolysis at $10.7\ s^{-1}$, followed by rapid ADP release at $>185\ s^{-1}$.

Short Processive Runs of Eg5—The results presented here do not define the point in the cycle where Eg5 is most likely to terminate its processive run. However, we speculate that the short run lengths of dimeric Eg5 in comparison with kinesin are because of the inability of Eg5 to keep the motor domains out-of-phase such that both heads reach the ADP state simultaneously. This could occur at steps 3–5 (Fig. 6) if ATP were to bind and hydrolyze at the forward head prematurely, or at steps 6 and 7 if ATP were hydrolyzed on the rearward head with ADP remaining at the forward head. The geometry or structural state of the neck linker may also play a role in loss of coordination and motor detachment (43). These are but two of a number of possibilities. We propose that the head-head communication of the Eg5 dimer leads to the short run lengths observed experimentally, and this behavior may be required for the functional roles of the Eg5 tetramer in the spindle. This type of mechanism may prevent the homotetramer from stalling at a roadblock by terminating the processive run on one microtubule with Eg5 remaining attached to the other MT. This behavior may also permit MT dynamics promoted by other proteins and/or kinesin motors and may be essential to achieve the balance of plus-end and minus-end directed forces for the metaphase spindle.

Although this study provides a mechanistic understanding of Eg5 mechanochemistry and head-head communication, one intriguing question ahead is to understand the mechanistic advantage of one rate-limiting transition to establish the processive run and another, rate-limiting ATP hydrolysis, to control the velocity of the processive run.

Acknowledgments—We thank Drs. Smita Patel and Gui-Zing Tang for the use of their fluorimeter and for assistance with the mantADP titrations; Dr. Jared Cochran for Eg5-367$_{NF}$; Yuanyuan Duan for her contribution to work with R234K; and members of the Gilbert lab. We recognize the contributions of Dr. Michael Ostap who served as the external member of doctoral committee for T. C. K. Dr. Ostap also provided a number of suggestions and critical comments during this study. Finally, we acknowledge the anonymous reviewer who provided insightful comments about the E0 and E1 intermediates.

REFERENCES

1. Sawin, K. E., LeGuellec, K., Philippe, M., and Mitchison, T. J. (1992) *Nature* **359,** 540–543
2. Blangy, A., Lane, H. A., d'Herin, P., Harper, M., Kress, M., and Nigg, E. A. (1995) *Cell* **83,** 1159–1169
3. Kashina, A., Baskin, R. J., Cole, D., Wedaman, K., Saxton, W., and Scholey, J. (1996) *Nature* **379,** 270–272
4. Mayer, T. U., Kapoor, T. M., Haggarty, S. J., King, R. W., Schreiber, S. L., and Mitchison, T. J. (1999) *Science* **286,** 971–974
5. Sakowicz, R., Finer, J. T., Beraud, C., Crompton, A., Lewis, E., Fritsch, A., Lee, Y., Mak, J., Moody, R., Turincio, R., Chabala, J. C., Gonzales, P., Roth, S., Weitman, S., and Wood, K. W. (2004) *Cancer Res.* **64,** 3276–3280
6. DeBonis, S., Skoufias, D. A., Lebeau, L., Lopez, R., Robin, G., Margolis, R. L., Wade, R. H., and Kozielski, F. (2004) *Mol. Cancer Ther.* **3,** 1079–1090
7. Cox, C. D., Breslin, M. J., Mariano, B. J., Coleman, P. J., Buser, C. A., Walsh, E. S., Hamilton, K., Huber, H. E., Kohl, N. E., Torrent, M., Yan, Y., Kuo, L. C., and Hartman, G. D. (2005) *Bioorg. Med. Chem. Lett.* **15,** 2041–2045
8. Duhl, D. M., and Renhowe, P. A. (2005) *Curr. Opin. Drug Discov. Dev.* **8,** 431–436
9. Cole, D. G., Saxton, W. M., Sheehan, K. B., and Scholey, J. M. (1994) *J. Biol. Chem.* **269,** 22913–22916
10. Hoyt, M. A., He, L., Loo, K. K., and Saunders, W. S. (1992) *J. Cell Biol.* **118,** 109–120
11. Heck, M. M., Pereira, A., Pesavento, P., Yannoni, Y., Spradling, A. C., and Goldstein, L. S. (1993) *J. Cell Biol.* **123,** 665–679
12. Gaglio, T., Saredi, A., Bingham, J. B., Hasbani, M. J., Gill, S. R., Schroer, T. A., and Compton, D. A. (1996) *J. Cell Biol.* **135,** 399–414
13. Gordon, D. M., and Roof, D. M. (1999) *J. Biol. Chem.* **274,** 28779–28786
14. Sharp, D. J., McDonald, K. L., Brown, H. M., Matthies, H. J., Walczak, C., Vale, R., Mitchison, T. J., and Scholey, J. M. (1999) *J. Cell Biol.* **144,** 125–138
15. Sharp, D. J., Yu, K. R., Sisson, J. C., Sullivan, W., and Scholey, J. M. (1999) *Nat. Cell Biol.* **1,** 51–54
16. Mountain, V., Simerly, C., Howard, L., Ando, A., Schatten, G., and Compton, D. A. (1999) *J. Cell Biol.* **147,** 351–365
17. Kapoor, T. M., Mayer, T. U., Coughlin, M. L., and Mitchison, T. J. (2000) *J. Cell Biol.* **150,** 975–988
18. Wilde, A., Lizarraga, S. B., Zhang, L., Wiese, C., Gliksman, N. R., Walczak, C. E., and Zheng, Y. (2001) *Nat. Cell Biol.* **3,** 221–227
19. Goshima, G., and Vale, R. D. (2003) *J. Cell Biol.* **162,** 1003–1016
20. Cytrynbaum, E. N., Scholey, J. M., and Mogilner, A. (2003) *Biophys. J.* **84,** 757–769
21. Chakravarty, A., Howard, L., and Compton, D. A. (2004) *Mol. Biol. Cell* **15,** 2116–2132
22. Kwon, M., and Scholey, J. (2004) *Trends Cell Biol.* **14,** 194–205
23. Kwok, B. H., Yang, J. G., and Kapoor, T. M. (2004) *Curr. Biol.* **14,** 1783–1788
24. Miyamoto, D. T., Perlman, Z. E., Burbank, K. S., Groen, A. C., and Mitchison, T. J. (2004) *J. Cell Biol.* **167,** 813–818
25. Shirasu-Hiza, M., Perlman, Z. E., Wittmann, T., Karsenti, E., and Mitchison, T. J. (2004) *Curr. Biol.* **14,** 1941–1945
26. Goshima, G., and Vale, R. D. (2005) *Mol. Biol. Cell* **16,** 3896–3907
27. Mitchison, T. J., Maddox, P., Gaetz, J., Groen, A., Shirasu, M., Desai, A., Salmon, E. D., and Kapoor, T. M. (2005) *Mol. Biol. Cell* **16,** 3064–3076
28. Tao, L., Mogilner, A., Civelekoglu-Scholey, G., Wollman, R., Evans, J., Stahlberg, H., and Scholey, J. M. (2006) *Curr. Biol.* **16,** 2293–2302
29. Goshima, G., Wollman, R., Goodwin, S. S., Zhang, N., Scholey, J. M., Vale, R. D., and Stuurman, N. (2007) *Science* **316,** 417–421
30. Kapitein, L. C., Peterman, E. J., Kwok, B. H., Kim, J. H., Kapoor, T. M., and Schmidt, C. F. (2005) *Nature* **435,** 114–118
31. Hackney, D. D. (1994) *Proc. Natl. Acad. Sci. U. S. A.* **91,** 6865–6869
32. Gilbert, S. P., Webb, M. R., Brune, M., and Johnson, K. A. (1995) *Nature* **373,** 671–676
33. Ma, Y.-Z., and Taylor, E. W. (1997) *J. Biol. Chem.* **272,** 724–730
34. Gilbert, S. P., Moyer, M. L., and Johnson, K. A. (1998) *Biochemistry* **37,** 792–799
35. Krzysiak, T. C., and Gilbert, S. P. (2006) *J. Biol. Chem.* **281,** 39444–39454
36. Valentine, M. T., Fordyce, P. M., Krzysiak, T. C., Gilbert, S. P., and Block, S. M. (2006) *Nat. Cell Biol.* **8,** 470–476
37. Valentine, M. T., Fordyce, P. M., and Block, S. M. (2006) *Cell Div.* **1,** 31
38. Valentine, M. T., and Gilbert, S. P. (2007) *Curr. Opin. Cell Biol.* **19,** 75–81
39. Block, S. M., Goldstein, L. S. B., and Schnapp, B. J. (1990) *Nature* **348,** 348–352
40. Howard, J., Hudspeth, A. J., and Vale, R. D. (1989) *Nature* **342,** 154–158
41. Rosenfeld, S. S., Xing, J., Jefferson, G. M., and King, P. H. (2005) *J. Biol. Chem.* **280,** 35684–35695
42. Klumpp, L. M., Hoenger, A., and Gilbert, S. P. (2004) *Proc. Natl. Acad. Sci. U. S. A.* **101,** 3444–3449
43. Krzysiak, T. C., Wendt, T., Sproul, L. R., Tittmann, P., Gross, H., Gilbert, S. P., and Hoenger, A. (2006) *EMBO J.* **25,** 2263–2273
44. Cochran, J. C., Sontag, C. A., Maliga, Z., Kapoor, T. M., Correia, J. J., and Gilbert, S. P. (2004) *J. Biol. Chem.* **279,** 38861–38870
45. Cochran, J. C., and Gilbert, S. P. (2005) *Biochemistry* **44,** 16633–16648
46. Foster, K. A., Mackey, A. T., and Gilbert, S. P. (2001) *J. Biol. Chem.* **276,** 19259–19266
47. Patel, S. S., and Bandwar, R. P. (2003) *Methods Enzymol.* **370,** 668–686
48. Press, W., Flannery, B. P., Teukolsky, S. A., and Vetterling, W. T. (1997) *Numerical Recipes in C: The Art of Scientific Computing*, 2nd Ed., 994 pp., Cambridge University Place, New York
49. Hackney, D. D. (1988) *Proc. Natl. Acad. Sci. U. S. A.* **85,** 6314–6318
50. Gilbert, S. P., and Johnson, K. A. (1993) *Biochemistry* **32,** 4677–4684
51. Hackney, D. D., Stock, M. F., Moore, J., and Patterson, R. A. (2003) *Biochemistry* **42,** 12011–12018
52. Rice, S., Lin, A. W., Safer, D., Hart, C. L., Naber, N., Carragher, B. O., Cain, S. M., Pechatnikova, E., Wilson-Kubalek, E. M., Whittaker, M., Pate, E., Cooke, R., Taylor, E. W., Milligan, R. A., and Vale, R. D. (1999) *Nature* **402,** 778–784
53. Foster, K. A., and Gilbert, S. P. (2000) *Biochemistry* **39,** 1784–1791
54. Turner, J., Anderson, R., Guo, J., Beraud, C., Fletterick, R., and Sakowicz, R. (2001) *J. Biol. Chem.* **276,** 25496–25502
55. Yan, Y., Sardana, V., Xu, B., Homnick, C., Halczenko, W., Buser, C. A., Schaber, M., Hartman, G. D., Huber, H. E., and Kuo, L. C. (2004) *J. Mol. Biol.* **335,** 547–554
56. Guydosh, N. R., and Block, S. M. (2006) *Proc. Natl. Acad. Sci. U. S. A.* **103,** 8054–8059
57. Rosenfeld, S. S., Fordyce, P. M., Jeffereson, G. M., King, P. H., and Block, S. M. (2003) *J. Biol. Chem.* **278,** 18550–18556
58. Asenjo, A. B., Weinberg, Y., and Sosa, H. (2006) *Nat. Struct. Mol. Biol.* **13,** 648–654